# Efficient decoupling technique applied to the numerical time integration of advanced interaction models for railway dynamics

**J. Giner-Navarro[1] | J. Martínez-Casas[1] | F. D. Denia[1] | L. Baeza[2]**

[1]Centro de Investigación en Ingeniería Mecánica, Universitat Politècnica de València, Camino de Vera s/n, 46022 Valencia, Spain.

[2]Institute of Sound and Vibration Research, University of Southampton, Southampton SO17 1BJ, UK.

**Correspondence**

J. Giner-Navarro, Centro de Investigación en Ingeniería Mecánica, Universitat Politècnica de València, Camino de Vera s/n, 46022 Valencia, Spain.

E-mail: juanginer@upv.es

**ACKNOWLEDGEMENTS**

The authors gratefully acknowledge the financial support of Spanish Ministry of Economy, Industry and Competitiveness and the European Regional Development Fund (project TRA2017-84701-R), as well as Generalitat Valenciana (project Prometeo/2016/007) and European Commission through the project "RUN2Rail - Innovative RUNning gear soluTiOns for new dependable, sustainable, intelligent and comfortable RAIL vehicles" (Horizon 2020 Shift2Rail JU call 2017, grant number 777564).

## ABSTRACT

Railway interaction is characterised by the coupling between the train and the track introduced through the wheel/rail contact. The introduction of the flexibility in the wheelset and the track through the Finite Element (FE) method in the last four decades has permitted to study high-frequency phenomena such as rolling noise and squeal, whose origin lies in the strongly non-steady state and non-linear behaviour of the contact forces that arise from the small contact area. In order to address models with a large number of degrees of freedom, innovative Eulerian-modal models for wheelsets with rotation and cyclic tracks have been developed in recent years. The aim of this paper is to extend the resulting formulation to an uncoupled linear matrix equation of motion that allows solving each equation independently for each time step, considerably reducing the associated computational cost. The decoupling integration method proposed is compared in terms of computational performance with

Newmark and Runge-Kutta schemes, commonly used in vehicle dynamics, for simulations with the leading wheelset negotiating a tangent track and accounting the rail roughness.

**KEYWORDS**

Railway dynamics, rolling contact, decoupling technique, contact linearisation, computational performance

## 1 INTRODUCTION

Train/track interaction consists of the coupled vibration of a railway vehicle and a track coupling by the contact area between both wheels and the corresponding rails. From the small contact patch, non-steady state contact forces emerge in the normal and tangential directions characterised by its high levels and strong non-linear behaviour. Unwanted phenomena such as high levels of noise and vibration[1], damage of the rolling surfaces in the form of corrugation[2] or rolling contact fatigue[3] occur due to large levels of vibration and dynamic fluctuations of the contact forces.

In favour of getting closer to better understanding of the physics behind these phenomena, a large effort has been spent over the last forty years to develop suitable railway interaction models. Although early models simplify the vehicle as a rigid wheelset resting on a Hertzian stiffness[4], the incorporation of the flexibility[1,5] has led to widen the frequency range of analysis so as to get a more realistic representation of wheel/rail interaction effects at higher frequencies. Finite Element (FE) models have strongly entered in railways research to extend the frequency range above 1 kHz to address the rolling noise[6]. These models mesh the wheelset (or just the wheels) with a higher refinement around the contact zone, where the forces and displacements reach more significant values to obtain accurate results in the high-frequency domain. Only very recently, a further model enhance was introduced in the wheelset to consider the inertial effects due to wheelset rotation[7,8], which is revealed crucial for rail corrugation[9].

The rails have been widely represented by means of a continuous horizontal Bernoulli-Euler beams on periodic discrete elastic supports subjected to a moving load[10,11]. More sophisticated models make use of Timoshenko beam elements to include rotational inertia and shear deformation, but its frequency range is limited up to 1.5 kHz for the tangential vibrations since it does not account the cross-sectional deformation of the rail[1]. The mobile nature of the contact force along the rail leads to refine uniformly the entire solid in the longitudinal direction, accumulating a number of degrees of freedom computationally unviable. In order to extend the frequency range maintaining an acceptable number of degrees of freedom, the Moving Element (ME) method[12] is applied in the rail formulation. From an Eulerian approach, this technique permits to fix the contact force applied in the same node of the mesh and thus to refine the mesh just around this node.

Numerical strategies need to be applied in order to reduce the number of differential equations and the associated unknowns of the complete system. In general, a modal synthesis is introduced to lower the size of the problem[5]. Through the calculation of the natural frequencies and the mode shape functions matrices of each substructure, the physical coordinates are replaced by a reduced number of modal coordinates as unknowns. The resulting linear differential equations are coupled.

At this point, the aim of this paper is to propose a mathematical strategy that permits to decouple the equations of motion and allows solving each one independently for each time step, optimising the numerical time integration. Additionally, this formulation will be extended to the particular case of a linearised contact model, simplification widely used in the literature[13]. With the aim of reducing the computational complexity of the problem, one single flexible wheelset is considered instead of one complete bogie, and gravitational forces are prescribed at the primary suspension seats. A cyclic finite and flexible rail supported by a Winkler base using the ME method is also implemented.

Results for the proposed decoupling technique consist of the evaluation of the time consumption and the discrepancy associated with this method compared with other integration schemes commonly adopted in vehicle dynamics: Newmark and *ode45*. Newmark method[14] is an algorithm commonly used in rigid solid dynamic applications that has been extended for flexible substructures in the railway field with the aim that the user is able to set a constant time step suitable for the conditions and the frequency domain of the dynamic problem. *ode45* is a medium order method with variable time step based on Runge-Kutta scheme[15] recommended in the literature for solving equations of motion associated with flexible substructures. These schemes are used for simulations run with a growing number of modes, permitting to corroborate the computational advantages of the proposed strategy for railway interaction models.

The paper presents the formulation of the flexible and rotating wheelset model and the ME technique applied to a cyclic rail (both in modal coordinates) in Section 2. Section 3 develops the decoupling technique for the complete dynamic interaction so as to obtain a reduced set of independent linear differential equations; this formulation is extended to the case of linear contact model. The computational performance of the proposed solver is evaluated through the discrepancy, the time consumption and the number of modal coordinates in Section 4. The paper closes with conclusive remarks in Section 5.

## 2 WHEELSET AND TRACK MODELS

### 2.1 Modal synthesis

A substructuring technique is followed in this paper for the vehicle/track interaction model[16,17], permitting to divide the whole system into two substructures: the vehicle and the track, being the wheel/rail contact forces that couple the equations of motion of both substructure. The physical matrix equation of motion for both of them can be written as

$$\mathbf{M}_{eq}^{i}\,\ddot{\mathbf{w}}^{i}+\mathbf{C}_{eq}^{i}\,\dot{\mathbf{w}}^{i}+\mathbf{K}_{eq}^{i}\,\mathbf{w}^{i}=\mathbf{F}^{i},\quad i=w,r, \tag{1}$$

where $\mathbf{M}_{eq}^{i}$, $\mathbf{C}_{eq}^{i}$ and $\mathbf{K}_{eq}^{i}$ are the mass, damping and stiffness equivalent matrices, $\mathbf{F}^{i}$ is the external force vector and $i$ is referred to the wheelset ($w$) or the rails ($r$). The dimension of the equation of motion corresponds to the number of degrees of freedom of each substructure $N^i$, three times (longitudinal, lateral and vertical displacements) the number of nodes of the mesh.

A modal synthesis approach is applied to the previous equation, permitting to reduce the dimension to a significantly lower number of modal coordinates $m^i$. In order to address this approach, the eigenproblem associated with the undamped and non-excited system is solved for the wheelset subjected by the primary suspensions and the rail supported by a Winkler bedding. It allows calculating the first $m^i$ eigenvalues (the square of the first natural frequencies of the system) and their corresponding eigenvectors (or mode shape functions). The eigenvectors form the respective mode shape functions matrices $\mathbf{\Phi}^{i}$ with dimension $N^i \times m^i$. Both modal equations of motion are written as

$$\ddot{\mathbf{q}}^{i}+\tilde{\mathbf{C}}_{eq}^{i}\,\dot{\mathbf{q}}^{i}+\tilde{\mathbf{K}}_{eq}^{i}\,\mathbf{q}^{i}=\tilde{\mathbf{Q}}^{i},\quad i=w,r, \tag{2}$$

where the modal matrices are:

$$\tilde{\mathbf{K}}_{eq}^{i}=\mathbf{\Phi}^{i\mathrm{T}}\mathbf{K}_{eq}^{i}\mathbf{\Phi}^{i}, \tag{3}$$

$$\tilde{\mathbf{C}}_{eq}^{i}=\mathbf{\Phi}^{i\mathrm{T}}\mathbf{C}_{eq}^{i}\mathbf{\Phi}^{i}, \tag{4}$$

$$\tilde{\mathbf{Q}}^{i}=\mathbf{\Phi}^{i\mathrm{T}}\mathbf{F}^{i}. \tag{5}$$

Therefore, both modal matrices present $m^i \times m^i$ dimension and Equation (2) is a differential system of $m^i$ equations. Since the physical matrix $\mathbf{K}_{eq}^{i}$ from which the eigenproblem was solved is not symmetric, $\tilde{\mathbf{K}}_{eq}^{i}$ is not a diagonal matrix; $\mathbf{C}_{eq}^{i}$ is a general damping matrix and its corresponding modal matrix $\tilde{\mathbf{C}}_{eq}^{i}$ is also not diagonal. Therefore, it leads to a system of $m^i$ coupled modal differential equations, which is computationally more costly to solve.

## 2.2 Wheelset model

The wheelsets confined in a bogie are mostly subjected to dynamic forces from the train/track interaction in a range above 20 Hz, frequency range in which the mechanical filter introduced by the suspensions effectively isolates the sprung masses (bogie frame and carbody) from the motion of the unsprung masses (wheelsets and axle boxes). This permits simplifying the modelling of the vehicle through one single flexible wheelset instead of one complete vehicle so as to simplify the computational problem, together with the primary suspension (where the forces are prescribed) represented using viscoelastic lumped parameter elements.

In order to model the kinematics of the flexible wheelset, two configurations (undeformed and deformed) are defined (see Figure 1). The undeformed configuration is associated with the spinning velocity of the wheelset (at constant angular velocity). The deformed configuration considers the flexibility and small rigid solid displacements. The displacement field relates the deformed configuration with the undeformed configuration as it will be shown in Equation (6). The coordinates that are implemented in the wheelset model do not follow the material points of the solid which is the commonest procedure in Mechanics, nevertheless they are associated with spatial points (Eulerian approach). Let **u** an Eulerian vector coordinate in a fixed coordinate frame. Any property of the solid corresponds to the material point of the solid whose undeformed configuration is in the spatial point **u** at instant *t*. Following this criterion, the displacement field is defined by means of the following formula:

$$\mathbf{r} = \mathbf{u} + \mathbf{w}\left(\mathbf{u}, t\right), \tag{6}$$

where **r** is the final position of the particle, and **w** is the displacements associated with flexibility and small rigid body displacements. Due to the axisymmetric geometry of the wheelset, this methodology permits to represent the displacements in the spatial points from the non-deformed configuration using the vibration modes as basis in the fixed reference frame. These modes are calculated through the Finite Elements (FE) method. The resulting modal equation of motion for the selected wheelset is[18]:

$$\ddot{\mathbf{q}}^{w} + 2\Omega\,\tilde{\mathbf{V}}^{w}\dot{\mathbf{q}}^{w} + \left(\Omega^{2}\left(\tilde{\mathbf{A}}^{w} - \tilde{\mathbf{C}}^{w}\right) + \tilde{\mathbf{D}}^{w}\right)\mathbf{q}^{w} = \Omega^{2}\,\tilde{\mathbf{c}}^{w} + \tilde{\mathbf{Q}}_{c}^{w} + \tilde{\mathbf{Q}}_{s}^{w}, \tag{7}$$

where $\mathbf{q}^{w}$ is the modal coordinate vector and $\Omega$ the angular velocity of the wheelset. The matrix $\tilde{\mathbf{V}}^{w}$ can be identified as inertial force due to Coriolis acceleration associated with the convective velocity; $\tilde{\mathbf{A}}^{w}$ is related to convective acceleration; $\tilde{\mathbf{C}}^{w}$ is associated with centrifugal forces that appear after deformation of the solid; the diagonal matrix $\tilde{\mathbf{D}}^{w} = \mathrm{diag}\left(\omega_{r}^{2}\right)$ is the modal stiffness matrix that contains the square of the undamped natural frequencies of the free-boundary wheelset; column vector $\tilde{\mathbf{c}}^{w}$ corresponds to constant centrifugal forces; finally, $\tilde{\mathbf{Q}}_{c}^{w}$ and $\tilde{\mathbf{Q}}_{s}^{w}$ are the column vectors of the

modal generalised forces acting on the flexible wheelset resulting respectively from wheel/rail contact forces and from the forces applied by the primary suspension. A complete description of the wheelset formulation can be found in Reference[18].

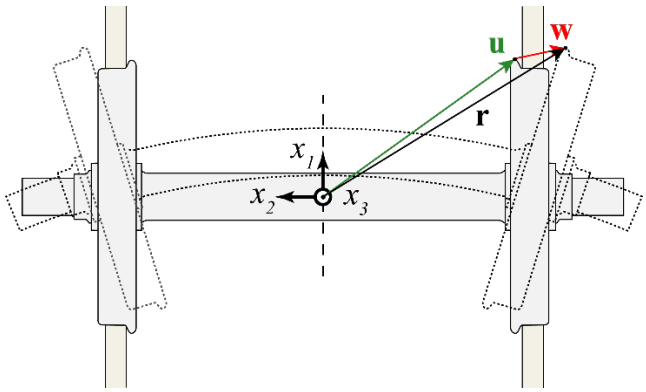


**FIGURE 1** Undeformed and deformed configuration of the wheelset negotiating a tangent track

### 2.3 Track model

A track model with cyclic conditions was developed in Reference[19] adopting the ME technique[12]. This method takes a moving frame attached to the vehicle, defining a new class of finite elements that makes the material of the rail 'flow' into the mesh. This model avoids the moving vehicle exceeding the 'downstream' boundary end since the vehicle (and the contact patch) remains fixed on a unique moving rail element instead of crossing from one element into another, hence avoiding the update of the force or displacement vectors. Furthermore, a fixed contact area permits to implement a mesh with greater refinement only around this area, where forces and displacements are more pronounced, avoiding to refine the entire head rail surface. As a finite element technique, ME method permits to account the cross-sectional deformation unlike beam models, hence widening the frequency range of validity.

The track model follows a cyclic approach[16], in which an infinite track negotiated by an infinite number of identical vehicles separated uniformly by a distance $L$ (set large enough to avoid the dynamic interaction between the vehicles) and travels at the same velocity $V$. Therefore, the study of the infinite track is reduced to a single section with finite length $L$ due to the periodicity of the structure and load conditions. Cyclic boundary conditions set same displacements and derivatives at the model edges of the finite rail.

A UIC60 profile is meshed and longitudinally extruded as seen in Figure 2 (out of scale). The governing equation is formulated in a relative reference system attached to the vehicle moving with velocity $V$. Again, an Eulerian-modal approach is adopted, so that the global displacement vector can be expressed through superposition of mode shapes. It must be pointed out that the mode shape functions do not depend on time since the 'flow' of the mesh through the material coordinates does

not change the mode shape functions in spatial coordinates because the cross-sectional area remains invariable after the extrusion of the UIC60 profile.

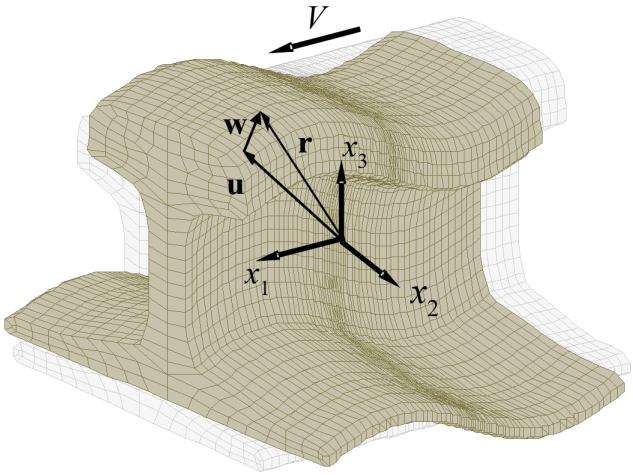


**FIGURE 2** Finite element mesh of the UIC60 rail (out of scale). Deformed and undeformed configuration

An Eulerian position vector **u** defined through the coordinate system $x_1x_2x_3$ is considered. Vector **u** defines the position of a spatial point and it does not depend on time. Vector $\mathbf{w} \equiv \mathbf{w}(\mathbf{u},t)$ is the displacement of a material point that occupies the position **u** at the instant $t$ with respect the undeformed configuration. The position vector of the material point is

$$\mathbf{r} = \mathbf{u} + \mathbf{w}(\mathbf{u},t). \tag{8}$$

The equation of motion in modal coordinates that governs the dynamic of the rail is the following:

$$\ddot{\mathbf{q}}^r + \left(\tilde{\mathbf{C}}^r_\zeta + \tilde{\mathbf{C}}^r_{wink} - 2V\,\tilde{\mathbf{C}}^r\right)\dot{\mathbf{q}}^r + \left(\tilde{\mathbf{D}}^r + \tilde{\mathbf{K}}^r_{wink} - V^2\tilde{\mathbf{A}}^r + V\,\tilde{\mathbf{K}}^r_{\mathbf{C}wink}\right)\mathbf{q}^r = \tilde{\mathbf{Q}}^r_c. \tag{9}$$

$\mathbf{q}^r$ is the modal coordinate vector, $\tilde{\mathbf{D}}^r$ is the modal stiffness, $\tilde{\mathbf{C}}^r_\zeta$ is a modal damping matrix included as recommended in the literature[1], $\tilde{\mathbf{A}}^r$ is related to the convective acceleration, $\tilde{\mathbf{C}}^r$ is a term associated with the convective velocity, $\tilde{\mathbf{K}}^r_{wink}$, $\tilde{\mathbf{K}}^r_{\mathbf{C}wink}$ and $\tilde{\mathbf{C}}^r_{wink}$ are terms that add the contribution of the Winkler bedding, and $\tilde{\mathbf{Q}}^r_c$ is the modal generalised force vector from wheel/rail contact. A complete description of the rail formulation can be found in Reference[19].

### 2.4 Wheelset/track interaction model

The wheelset and the rails are in contact (see Figure 3) and its equations of motion (7) and (9) are coupled through the wheel/rail contact forces in modal coordinates, identified as $\tilde{\mathbf{Q}}^w_c$ and $\tilde{\mathbf{Q}}^r_c$, respectively. The position and velocity of the contact points on the surfaces of both inner and outer

wheels and rails are determined in each time step to calculate the relative wheel/rail motion required for the computation of the normal and tangential contact force. This force expressed in Eulerian modal coordinates is applied on the wheel and the rail surfaces at the contact point. The general contact formulation for a generic track is detailed above.

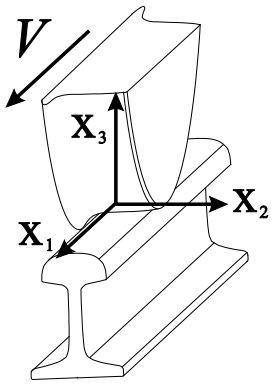


**FIGURE 3** Reference system used in the contact

### 2.4.1 Normal contact model

The normal contact problem is solved using an incremental approach. A pre-processor of a commercial vehicle/track interaction software based on multibody techniques is used to compute the quasi-static solution of the railway interaction model and the corresponding contact force applied to the contact point. This software considers elastic contact, permitting to determine a single contact point on each wheel/rail pair assuming both wheel and rail undeformable and computing the relative lateral displacement of the wheel on the rail. The lateral displacement will be considered as mean value around which the contact point will oscillate during the numerical integration assuming small variations.

The contact displacements associated with the wheel and the rail, $\mathbf{w}_c^w$ and $\mathbf{w}_c^r$, respectively, are calculated through the modal superposition principle. The wheel/rail incremental distance vector is computed assuming that both surfaces are undeformable:

$$\mathbf{\Delta} = \mathbf{w}_c^r - \mathbf{w}_c^w. \tag{10}$$

The quasi-static normal contact force permits to estimate the corresponding approach $\bar{\delta}$ through Hertzian theory[20]:

$$\bar{\delta} = \left( \frac{\bar{F}_3}{K_H} \right)^{2/3}, \tag{11}$$

where $K_H$ is a contact stiffness estimated from the material properties and curvatures in the contact point[21], and $\overline{F}_3$ is the quasi-static normal contact force. The incremental approach is obtained by projecting the distance $\boldsymbol{\Delta}$ along the direction normal to the contact plane:

$$\Delta\delta = \boldsymbol{\Delta}^{\mathrm{T}}\mathbf{x}_3\,, \tag{12}$$

where $\mathbf{x}_3$ is the unit normal vector (see Figure 3). The total normal force in the contact area $F_3$ at each time step for the numerical integration can finally be estimated using again Equation (11) after adding the incremental approach to the quasi-static one:

$$F_3 = \overline{F}_3 + \Delta F_3 = \begin{cases} K_H\left(\overline{\delta} + \Delta\delta\right)^{3/2} & \text{if } \left(\overline{\delta} + \Delta\delta\right) > 0, \\ 0 & \text{if } \left(\overline{\delta} + \Delta\delta\right) \le 0. \end{cases} \tag{13}$$

The contact area and the normal traction distribution are obtained by means of the Hertzian contact model[20] from the normal force $F_3$.

### 2.4.2 Tangential contact model

The tangential contact problem is solved by implementing Kalker's algorithm CONTACT[22]. Again, an incremental approach is adopted assuming small variations of the creepages around the quasi-static longitudinal $\overline{\xi}_1$, lateral $\overline{\xi}_2$ and spin $\overline{\xi}_{sp}$ values provided by the multibody software:

$$\xi_1 = \frac{1}{V}\dot{\boldsymbol{\Delta}}^{\mathrm{T}}\,\mathbf{x}_1 + \overline{\xi}_1, \tag{14}$$

$$\xi_2 = \frac{1}{V}\dot{\boldsymbol{\Delta}}^{\mathrm{T}}\,\mathbf{x}_2 + \overline{\xi}_2, \tag{15}$$

$$\xi_{sp} = \overline{\xi}_{sp}, \tag{16}$$

where $\mathbf{x}_1$ and $\mathbf{x}_2$ are unit vectors in the rolling and lateral direction, respectively (see Figure 3). Following the non-steady CONTACT algorithm, the computation of the tangential traction distribution also depends on the displacements produced in the present mesh by the computed traction in the previous instant of the numerical integration. The longitudinal and lateral contact forces, $F_1$ and $F_2$ respectively, are estimated and, together with the normal one $F_3$, projected along the inertial coordinate system for the wheelset and the track, accounting for the inclination of the wheel/rail contact plane. Finally, the resulting projections are applied in both wheels and the rails (with opposite sign) in the corresponding contact points as external actions, providing the generalised force vectors

in modal coordinates associated with the contact forces, $\tilde{\mathbf{Q}}_c^w$ and $\tilde{\mathbf{Q}}_c^r$, included in Equations (7) and (9), respectively.

### 2.4.3 Coupled wheelset/track equations of motion

The equations of motion for the coupled wheelset/track system are assembled by considering Equation (7) for the rotating wheelset and Equation (9) for both inner and outer rails supported by a uniform viscoelastic Winkler bedding:

$$
\begin{aligned}
&\begin{pmatrix} \ddot{\mathbf{q}}^w \\ \ddot{\mathbf{q}}_{inn}^r \\ \ddot{\mathbf{q}}_{out}^r \end{pmatrix} + \begin{pmatrix} 2\Omega\,\tilde{\mathbf{V}}^w & \mathbf{0} & \mathbf{0} \\ \mathbf{0} & -2V\tilde{\mathbf{C}}^r + \tilde{\mathbf{C}}_{wink}^r + \tilde{\mathbf{C}}_{\zeta}^r & \mathbf{0} \\ \mathbf{0} & \mathbf{0} & -2V\tilde{\mathbf{C}}^r + \tilde{\mathbf{C}}_{wink}^r + \tilde{\mathbf{C}}_{\zeta}^r \end{pmatrix} \begin{pmatrix} \dot{\mathbf{q}}^w \\ \dot{\mathbf{q}}_{inn}^r \\ \dot{\mathbf{q}}_{out}^r \end{pmatrix} \\
&+ \begin{pmatrix} \Omega^2\left(\tilde{\mathbf{A}}^w - \tilde{\mathbf{C}}^w\right) + \tilde{\mathbf{D}}^w & & \\ & \mathbf{0} & \\ & & \mathbf{0} \end{pmatrix} \\
&\begin{pmatrix} \tilde{\mathbf{D}}^r - V^2\tilde{\mathbf{A}}^r + \tilde{\mathbf{K}}_{wink}^r + V\tilde{\mathbf{K}}_{\mathbf{C}wink}^r & \mathbf{0} & \mathbf{0} \\ \mathbf{0} & \tilde{\mathbf{D}}^r - V^2\tilde{\mathbf{A}}^r + \tilde{\mathbf{K}}_{wink}^r + V\tilde{\mathbf{K}}_{\mathbf{C}wink}^r & \mathbf{0} \\ \mathbf{0} & \mathbf{0} & \tilde{\mathbf{D}}^r - V^2\tilde{\mathbf{A}}^r + \tilde{\mathbf{K}}_{wink}^r + V\tilde{\mathbf{K}}_{\mathbf{C}wink}^r \end{pmatrix} \begin{pmatrix} \mathbf{q}^w \\ \mathbf{q}_{inn}^r \\ \mathbf{q}_{out}^r \end{pmatrix} = \\
&\begin{pmatrix} \ddot{\mathbf{q}}^w \\ \ddot{\mathbf{q}}_{inn}^r \\ \ddot{\mathbf{q}}_{out}^r \end{pmatrix} + \begin{pmatrix} \tilde{\mathbf{C}}_{eq}^w & \mathbf{0} & \mathbf{0} \\ \mathbf{0} & \tilde{\mathbf{C}}_{eq}^r & \mathbf{0} \\ \mathbf{0} & \mathbf{0} & \tilde{\mathbf{C}}_{eq}^r \end{pmatrix} \begin{pmatrix} \dot{\mathbf{q}}^w \\ \dot{\mathbf{q}}_{inn}^r \\ \dot{\mathbf{q}}_{out}^r \end{pmatrix} + \begin{pmatrix} \tilde{\mathbf{K}}_{eq}^w & \mathbf{0} & \mathbf{0} \\ \mathbf{0} & \tilde{\mathbf{K}}_{eq}^r & \mathbf{0} \\ \mathbf{0} & \mathbf{0} & \tilde{\mathbf{K}}_{eq}^r \end{pmatrix} \begin{pmatrix} \mathbf{q}^w \\ \mathbf{q}_{inn}^r \\ \mathbf{q}_{out}^r \end{pmatrix} \\
&= \ddot{\mathbf{q}}^{wr} + \tilde{\mathbf{C}}^{wr}\dot{\mathbf{q}}^{wr} + \tilde{\mathbf{K}}^{wr}\mathbf{q}^{wr} = \tilde{\mathbf{Q}}_c^{wr},
\end{aligned}
\tag{17}
$$

where $\mathbf{q}^{wr} = \left(\mathbf{q}^w, \mathbf{q}_{inn}^r, \mathbf{q}_{out}^r\right)^{\mathrm{T}}$ and $\tilde{\mathbf{Q}}_c^{wr} = \left(\Omega^2\tilde{\mathbf{c}}^w + \tilde{\mathbf{Q}}_c^w + \tilde{\mathbf{Q}}_s^w, \tilde{\mathbf{Q}}_{c,inn}^r, \tilde{\mathbf{Q}}_{c,out}^r\right)^{\mathrm{T}}$. The subscripts *inn* and *out* refer to the internal and external rail, respectively.

## 3 EFFICIENT NUMERICAL STRATEGY

### 3.1 Decoupling technique

Equation (17) is a linear differential system coupled by the generalised contact forces $\tilde{\mathbf{Q}}_c^{wr}$. The following strategy permits to obtain uncoupled linear differential equations through an efficient modal mechanism based on two variable transformations applied in the pre-process. Equation (17) is cast into first-order (state-space) form as:

$$
\tilde{\mathbf{A}}^{wr}\dot{\boldsymbol{\theta}}^{wr} + \tilde{\mathbf{B}}^{wr}\boldsymbol{\theta}^{wr} = \begin{Bmatrix} \tilde{\mathbf{Q}}_c^{wr} \\ \mathbf{0} \end{Bmatrix},
\tag{18}
$$

where

$$\tilde{\mathbf{A}}^{wr} = \begin{pmatrix} \tilde{\mathbf{C}}^{wr} & \mathbf{I} \\ \mathbf{I} & \mathbf{0} \end{pmatrix}, \quad \tilde{\mathbf{B}}^{wr} = \begin{pmatrix} \tilde{\mathbf{K}}^{wr} & \mathbf{0} \\ \mathbf{0} & -\mathbf{I} \end{pmatrix}, \quad \boldsymbol{\theta}^{wr} = \begin{pmatrix} \mathbf{q}^{wr} \\ \dot{\mathbf{q}}^{wr} \end{pmatrix}. \tag{19}$$

The new variable $\boldsymbol{\theta}^{wr}$ is a vector of length $2m$, where $m = m^{w} + 2m^{r}$ is the number of modal coordinates considered for the wheelset/track system. Note that $\left(\tilde{\mathbf{A}}^{wr}\right)^{-1} \tilde{\mathbf{B}}^{wr}$ is

$$\left(\tilde{\mathbf{A}}^{wr}\right)^{-1} \tilde{\mathbf{B}}^{wr} = \begin{pmatrix} \mathbf{0} & -\mathbf{I} \\ \tilde{\mathbf{K}}^{wr} & \tilde{\mathbf{C}}^{wr} \end{pmatrix}. \tag{20}$$

Solving the eigenproblem from the matrix $\left(\tilde{\mathbf{A}}^{wr}\right)^{-1} \tilde{\mathbf{B}}^{wr}$ without truncation, it is obtained $m$ conjugated pairs of eigenvectors $\{\xi\}_i$ and eigenvalues $\lambda_i$. The eigenmatrix results $\boldsymbol{\Xi} = \left(\{\xi\}_i, \{\xi\}_i^{*}, \ldots\right)$ and the eigenvalues diagonal matrix $\boldsymbol{\lambda} = \mathrm{diag}\left(\lambda_i, \lambda_i^{*}, \ldots\right)$, where $i = 1, \ldots m$. From the definition of the eigenvectors calculated:

$$\boldsymbol{\Xi}^{-1} \left( \left(\tilde{\mathbf{A}}^{wr}\right)^{-1} \tilde{\mathbf{B}}^{wr} \right) \boldsymbol{\Xi} = \boldsymbol{\lambda}. \tag{21}$$

A new transformation is adopted at this point, so that the modal vector $\boldsymbol{\theta}^{wr}$ can be expressed through the eigenvectors matrix $\boldsymbol{\Xi}$ and a new modal coordinates vector $\mathbf{s}$:

$$\boldsymbol{\theta}^{wr} = \boldsymbol{\Xi}\, \mathbf{s}. \tag{22}$$

Replacing Equation (22) in Equation (18), pre-multiplying by $\boldsymbol{\Xi}^{-1}$ and considering the relationship expressed in Equation (21), the linear first-order coupled equation system becomes in a decoupled equation system since $\boldsymbol{\lambda}$ is a diagonal matrix:

$$\dot{\mathbf{s}} + \boldsymbol{\lambda}\, \mathbf{s} = \tilde{\mathbf{G}}, \tag{23}$$

where

$$\tilde{\mathbf{G}} = \boldsymbol{\Xi}^{-1} \left(\tilde{\mathbf{A}}^{wr}\right)^{-1} \begin{Bmatrix} \tilde{\mathbf{Q}}_c^{wr} \\ \mathbf{0} \end{Bmatrix}. \tag{24}$$

The unknowns of Equation (23) can be separated in $2m$ independent equations, simplifying hugely the solving procedure:

$$\left.\begin{aligned}\dot{s}_\iota + \lambda_\iota s_\iota &= \tilde{G}_\iota \\ \dot{s}_\iota + \lambda_\iota^* s_\iota &= \tilde{G}_\iota^*\end{aligned}\right\}, \quad \iota = 1, \ldots m. \tag{25}$$

At this point, the computational cost can be halved by removing the conjugated pairs of $\boldsymbol{\Xi} = \left(\{\xi\}_i, \{\xi\}_i^*, \ldots\right)$ and $\boldsymbol{\lambda} = \mathrm{diag}\left(\lambda_i, \lambda_i^*, \ldots\right)$:

$$\boldsymbol{\Theta} = \left(\{\xi\}_1, \ldots \{\xi\}_m\right), \tag{26}$$

$$\boldsymbol{\Gamma} = \mathrm{diag}\left(\lambda_1, \ldots \lambda_m\right). \tag{27}$$

Hence, instead of the transformation expressed in Equation (22), an equivalent transformation after discarding the conjugated pairs is adopted:

$$\boldsymbol{\theta}^{wr} = \boldsymbol{\Theta}\mathbf{p}, \tag{28}$$

being $\mathbf{p}$ the new modal coordinates vector. Finally, Equation (25) of $2m$ independent equations is reduced to $m$ independent equations system:

$$\dot{p}_\iota + \lambda_\iota p_\iota = \tilde{H}_\iota, \quad \iota = 1, \ldots m, \tag{29}$$

where

$$\widetilde{\mathbf{H}} = \mathrm{pinv}\left(\boldsymbol{\Theta}\right)\left(\widetilde{\mathbf{A}}^{wr}\right)^{-1}\begin{Bmatrix}\widetilde{\mathbf{Q}}_c^{wr} \\ \mathbf{0}\end{Bmatrix}, \tag{30}$$

and *pinv* is the Moore-Penrose pseudoinverse for the non-square matrix $\boldsymbol{\Theta}$. The main advantage of getting a diagonalised formulation and, hence, decoupled linear first-order equations is that they can be solved analytically time step by time step through

$$p_\iota\left(t_{j+1}\right) = p_\iota\left(t_j\right)e^{-\lambda_\iota \Delta t} + \frac{\tilde{H}_\iota\left(t_j\right)}{\lambda_i}\left(1 - e^{-\lambda_\iota \Delta t}\right), \quad \iota = 1, \ldots m, \tag{31}$$

where $t_{j+1} = t_j + \Delta t$.

### 3.2 Static modal correction

This section presents the formulation of a technique considered in this work that corrects the static gain shift of the solution from the truncation effectuated in the modal approach, hence leading to a loss of information as a consequence of the reduction of the number of state variables (modal

coordinates). This technique estimates the deviation in the static solution between the non-reduced procedure and the modal transformation.

The solving methodology based on the modal approach gives an approximated stiffness matrix $\mathbf{K}^{i}_{eq,\mathrm{m}}$, introducing a small but non-negligible deviation with respect to the original stiffness matrix in physical coordinates $\mathbf{K}^{i}_{eq}$ (see Equation (1)). This deviation is the responsible for the static discrepancy introduced by the modal approach in the solution. The equivalent stiffness matrix $\mathbf{K}^{i}_{eq,\mathrm{m}}$ in physical coordinates can be computed from the modal stiffness matrix (see Equation (3)):

$$\mathbf{K}^{i}_{eq,\mathrm{m}} = \mathbf{\Phi}^{i}\,\tilde{\mathbf{K}}^{i}_{eq}\,\mathbf{\Phi}^{i\mathrm{T}}, \quad i = w, r. \tag{32}$$

From the previous expression, the static response in physical coordinates from the modal one is computed as

$$\mathbf{w}^{i}_{st,\mathrm{m}} = \left(\mathbf{K}^{i}_{eq,\mathrm{m}}\right)^{-1}\mathbf{F}^{i}, \quad i = w, r, \tag{33}$$

while the static response from the original stiffness matrix in physical coordinates is

$$\mathbf{w}^{i}_{st} = \left(\mathbf{K}^{i}_{eq}\right)^{-1}\mathbf{F}^{i}, \quad i = w, r. \tag{34}$$

The static modal correction, $\mathcal{G}^{i}$, is simply estimated as the difference between both approaches:

$$\mathcal{G}^{i} = \mathbf{w}^{i}_{st} - \mathbf{w}^{i}_{st,\mathrm{m}} = \left[\left(\mathbf{K}^{i}_{eq}\right)^{-1} - \left(\mathbf{K}^{i}_{eq,\mathrm{m}}\right)^{-1}\right]\mathbf{F}^{i}, \quad i = w, r. \tag{35}$$

This deviation can be easily corrected by adding the static modal correction in the computed solution from the modal technique:

$$\mathbf{w}^{i}_{corr} = \mathbf{w}^{i}_{\mathrm{m}} + \mathcal{G}^{i}. \tag{36}$$

Figure 4 shows how this term works satisfactorily for a 1D ME cyclic rail model based on Koh *et al.* formulation[12], implemented for UIC60 rail of 42 m of length supported by a uniform viscoelastic Winkler bedding (see Table 1). The model is uniformly meshed along the longitudinal direction using 100 beam elements. The rail is subjected to a vertical constant moving force of 56.1 kN applied in the contact point, corresponding to the middle node; no wheel/rail interaction is considered in this case. The 1D mesh is longitudinally uniform and it consists of 200 nodes. The vertical displacement in the contact node is plotted for 0.05 s: the dashed line has been simulated by solving the corresponding equation of motion for physic coordinates; the continuous line shows the solution solving the modal equation of motion using 50 vibration modes; the deviation in the steady-state response reached for

both simulations is compensated by the static modal correction vector, which adjusts the modal solution to the physic one (light-grey line).

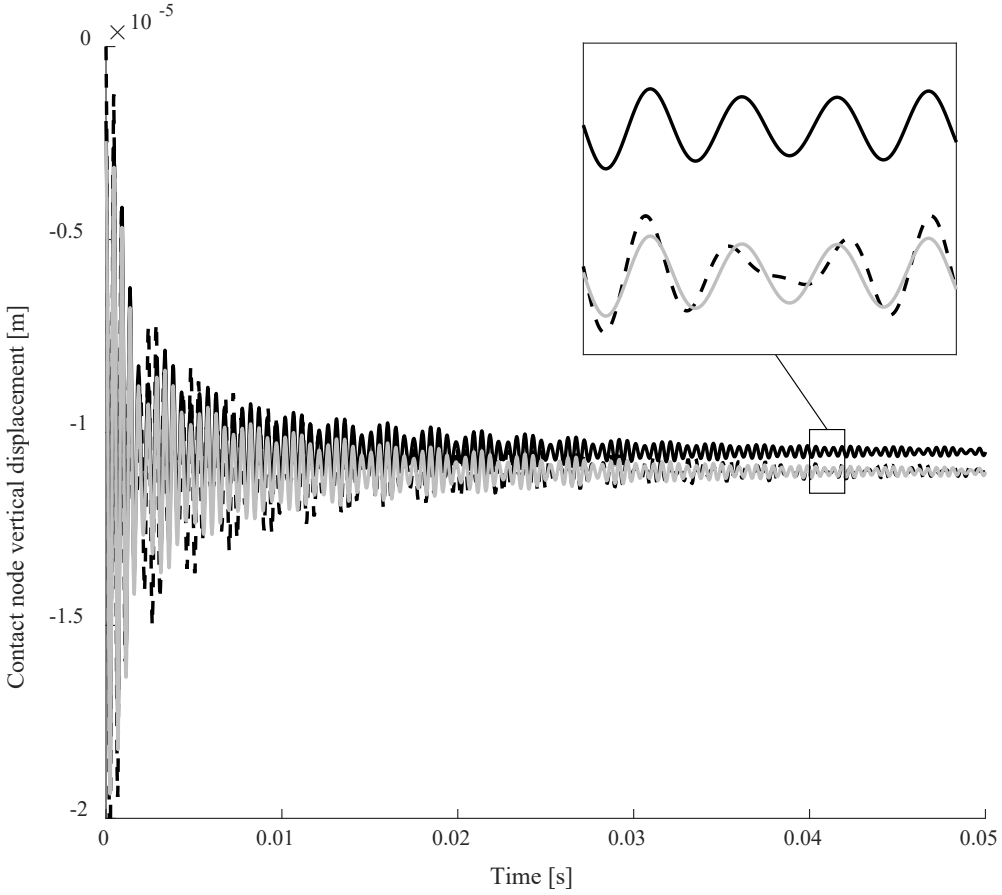


**FIGURE 4** Vertical displacement of the central node on the upper side of the 1D ME rail model. Results from: physic coordinates, 200 nodes (– – –); modal coordinates, 50 modes (———); modal coordinates, 50 modes, and compensated by the static modal correction $\mathcal{G}$ (———)

### 3.3 Contact linearisation

At this point, a numerical strategy is proposed in order to linearise and decouple the previous modal equations that describe the wheelset/track dynamic interaction. The contact force that couples both equations of motion for the wheelset and the rails is linearised around the quasi-static curving condition. Linearising Equation (13) around a mean value $\overline{\delta}$:

$$F_3 = K_H\big|_{lin}\,\delta, \tag{37}$$

where:

$$K_H\big|_{lin} = \frac{dF_3}{d\delta}\bigg|_{\bar{\delta}} = \frac{3}{2}K_H\bar{\delta}^{1/2} = \frac{3}{2}\frac{\bar{F}_3}{\bar{\delta}}. \tag{38}$$

The normal contact stiffness $K_H\big|_{lin}$ corresponds to the slope of the force-displacement curve obtained with the normal contact model at the vertical preload and it depends on the curvatures of wheel and rail surfaces at the contact. In order for Equation (37) to be introduced into modal equations, it is transformed into a generalised force vector. From Newton's third law, the following is obtained for the coupled wheel/rail system:

$$\tilde{\mathbf{Q}}_{c,n} = K_H\big|_{lin}\begin{pmatrix}\boldsymbol{\Phi}^w_{c,n} & \mathbf{0}\\ \mathbf{0} & \boldsymbol{\Phi}^r_{c,n}\end{pmatrix}^{\mathrm{T}}\begin{pmatrix}\boldsymbol{\Phi}^w_{c,n} & -\boldsymbol{\Phi}^r_{c,n}\\ -\boldsymbol{\Phi}^w_{c,n} & \boldsymbol{\Phi}^r_{c,n}\end{pmatrix}\begin{pmatrix}\mathbf{q}^w\\ \mathbf{q}^r\end{pmatrix}, \tag{39}$$

where $\boldsymbol{\Phi}^r_{c,n} = \mathbf{n}_c^{\mathrm{T}}\boldsymbol{\Phi}^r_c$, $\boldsymbol{\Phi}^w_{c,n} = \mathbf{n}_c^{\mathrm{T}}\boldsymbol{\Phi}^w_c$, $\boldsymbol{\Phi}^r_c$ and $\boldsymbol{\Phi}^w_c$ are the mode shapes in the degrees of freedom corresponding with the contact nodes of the rail and the wheel, $\mathbf{n}_c$ is the direction normal to the contact node and $\tilde{\mathbf{Q}}_{c,n}$ contains the generalised normal contact forces in the wheel and the rail. The external tangential generalised force vector is then calculated as:

$$\tilde{\mathbf{Q}}_{c,t} = \mu K_H\big|_{lin}\begin{pmatrix}\boldsymbol{\Phi}^w_{c,t} & \mathbf{0}\\ \mathbf{0} & \boldsymbol{\Phi}^r_{c,t}\end{pmatrix}^{\mathrm{T}}\begin{pmatrix}\boldsymbol{\Phi}^w_{c,n} & -\boldsymbol{\Phi}^r_{c,n}\\ -\boldsymbol{\Phi}^w_{c,n} & \boldsymbol{\Phi}^r_{c,n}\end{pmatrix}\begin{pmatrix}\mathbf{q}^w\\ \mathbf{q}^r\end{pmatrix}, \tag{40}$$

where $\boldsymbol{\Phi}^r_{c,t} = \mathbf{t}_c^{\mathrm{T}}\boldsymbol{\Phi}^r_c$, $\boldsymbol{\Phi}^w_{c,t} = \mathbf{t}_c^{\mathrm{T}}\boldsymbol{\Phi}^w_c$ and $\mathbf{t}_c$ is a unit vector acting in the plane of the wheel/rail contact in the direction given by the angle of attack. Taking into account that $\tilde{\mathbf{Q}}^{wr}_c = \left(\Omega^2\tilde{\mathbf{c}}^w + \tilde{\mathbf{Q}}_{c,n} + \tilde{\mathbf{Q}}_{c,t} + \tilde{\mathbf{Q}}^w_s, \tilde{\mathbf{Q}}^r_{c,inn}, \tilde{\mathbf{Q}}^r_{c,out}\right)^{\mathrm{T}}$ and considering the inner and outer rails, the homogenous equations of motion for the coupled wheel/rail system from Equation (17) are assembled:

$$\begin{pmatrix}\ddot{\mathbf{q}}^w\\ \ddot{\mathbf{q}}^r_{inn}\\ \ddot{\mathbf{q}}^r_{out}\end{pmatrix} + \begin{pmatrix}\tilde{\mathbf{C}}^w_{eq} & \mathbf{0} & \mathbf{0}\\ \mathbf{0} & \tilde{\mathbf{C}}^r_{eq} & \mathbf{0}\\ \mathbf{0} & \mathbf{0} & \tilde{\mathbf{C}}^r_{eq}\end{pmatrix}\begin{pmatrix}\dot{\mathbf{q}}^w\\ \dot{\mathbf{q}}^r_{inn}\\ \dot{\mathbf{q}}^r_{out}\end{pmatrix} + \begin{pmatrix}\tilde{\mathbf{K}}^w_{eq} + \tilde{\mathbf{k}}^{w,w}_{c,inn}\big|_{lin} + \tilde{\mathbf{k}}^{w,w}_{c,out}\big|_{lin} & -\tilde{\mathbf{k}}^{w,r}_{c,inn}\big|_{lin} & -\tilde{\mathbf{k}}^{w,r}_{c,out}\big|_{lin}\\ -\tilde{\mathbf{k}}^{r,w}_{c,inn}\big|_{lin} & \tilde{\mathbf{K}}^r_{eq} + \tilde{\mathbf{k}}^{r,r}_{c,inn}\big|_{lin} & \mathbf{0}\\ -\tilde{\mathbf{k}}^{r,w}_{c,out}\big|_{lin} & \mathbf{0} & \tilde{\mathbf{K}}^r_{eq} + \tilde{\mathbf{k}}^{r,r}_{c,out}\big|_{lin}\end{pmatrix}\begin{pmatrix}\mathbf{q}^w\\ \mathbf{q}^r_{inn}\\ \mathbf{q}^r_{out}\end{pmatrix} \tag{41}$$
$$= \ddot{\mathbf{q}}^{wr} + \tilde{\mathbf{C}}^{wr}\dot{\mathbf{q}}^{wr} + \tilde{\mathbf{K}}^{wr}\big|_{lin}\mathbf{q}^{wr} = \mathbf{0},$$

where $\mathbf{q}^{wr} = \left(\mathbf{q}^w, \mathbf{q}^r_{inn}, \mathbf{q}^r_{out}\right)^{\mathrm{T}}$ and

$$\tilde{\mathbf{k}}^{i,j}_{c,k}\big|_{lin} = -K_{H,k}\big|_{lin}\left(\boldsymbol{\Phi}^i_{(c,n),k} + \mu\boldsymbol{\Phi}^i_{(c,t),k}\right)^{\mathrm{T}}\boldsymbol{\Phi}^j_{(c,n),k}, \quad i = w,r; \quad j = w,r; \quad k = inn,out. \tag{42}$$

Equation (41) represents a linear non-symmetric (caused by inertia effects due to convective terms and the friction coupling) homogeneus matrix differential equation that can be computed as eigenvalue problem that is solved in the considered frequency range. Unstable eigenmodes of the coupled

train/track system are indicated by positive real-parts of the associated eigenvalues. The positive real-part gives the rate of growth of the vibration amplitude of the corresponding eigenmode.

This linearised formulation permits the computation of the wheelset/track system receptances from Equation (41) since the interaction between both substructures is included in the compact stiffness matrix. Additionally, the integration of Equation (41) in the time domain can be solved through an analytic expression after following the decoupling technique presented in Section 3.1. Nevertheless, it should be noted that the linearisation of the contact model is an unrealistic simplification only valid for low-medium frequency phenomena; problems associated with the high-frequency domain require a detailed 3D non-steady state and non-linear contact model so as to capture and reproduce their characteristics. Therefore, its computation is limited to a first approximation of the behaviour of the system considering the flexibility of its substructures in the low-medium frequency range.

## 4 NUMERICAL RESULTS

This section intends to exploit the computational advantages of the uncoupled linearised and non-linear formulations developed in Section 3 through a parametric study of time-domain simulations of a high-frequency railway interaction model implemented from the formulations described in Section 2 for the wheelset and the track. The model is evaluated for a vehicle running at 300 km/h through a tangent track. The case studied here refers to the trailed car of a concentrated power train for high speed passenger service. Only the leading wheelset is selected in this work, which is equipped with a solid axle wheelset with monobloc, the brake discs and light S1002 design wheels. The track considered features UIC60 (60 kg/m) rails and track parameters are based on the EUROBALT project[23], considering a "stiff" track. The friction coefficient is set at 0.40, which can be considered constant along the simulation[24]. Table 1 summarises the input data used to set up the simulation model.

**TABLE 1** Simulation parameters and properties

| **Wheelset model data** | | **Track model data** | |
|---|---|---|---|
| Mass of wheelset | 1375 kg | Rail section | UIC60 |
| Axle load | 120 kN | Rail length | 42 m |
| Primary suspension longitudinal stiffness | 7.5 MN/m | Track vertical bed stiffness | 43.7 MN/m |
| Primary suspension lateral stiffness | 7.1 MN/m | Track vertical bed damping | 12.6 kN s/m |
| Primary suspension vertical stiffness | 0.81 MN/m | | |
| Primary suspension longitudinal damping | 100 kN s/m | | |
| Primary suspension lateral damping | 100 kN s/m | | |
| Primary suspension vertical damping | 30 kN s/m | | |

The numerical time integration scheme Equation (31) deduced from the matrix equation of motion (17) for the wheelset/track interaction is evaluated in terms of computational performance by comparison with two different methods widely used in vehicle dynamics: Newmark scheme and a particular Runge-Kutta implementation. Newmark method has been adopted in previous works focused on high-frequency railway phenomena such as rail corrugation and wheelflats[18]. In agreement with simulations run, time integration strongly required small time steps to ensure the robustness of the numerical convergence due to the complexity of the instationary and non-linear contact model adopted, so that a fixed time step of $5\times10^{-6}$ s is used[25]. The Runge-Kutta method is applied through the *ode45* solver provided by Matlab© with adaptive time steps. Its numerical solution is set as the reference one so as to evaluate the error of the previous schemes in terms of discrepancy between solutions. The discrepancy is evaluated in the node in which the contact force is applied; the reference magnitude will be the norm of its displacement solution along the simulation, computed from *ode45* considering the maximum number of mode shapes for each case of study. Since the largest deformation field will be registered at this point, the registered discrepancy will be more appropriate for the numerical evaluation.

These three schemes are used for solving the dynamics of the track through the numerical time integration of its equation of motion in modal coordinates (Equation (9)) and the wheelset/track dynamic interaction (Equation (17). The modal truncation, together with the static modal correction defined in Section 3.2, permits to reduce the system dimension, making the problem computationally approachable with a conventional PC. A parameter study for the three schemes under research is carried out, evaluating the time consumption for a total simulation time of 1 s and the discrepancy with respect to the reference solution. In this work, the simulations are run through a PC with the following specifications: Intel(R) Core(TM) i5-2500 CPU @ 3.30GHz with 8.00 GB of RAM and 64-bit computing.

This section is divided into three subsections. Sections 4.1 and 4.2 show the simulation results computed for the numerical performance of the decoupling method proposed in Equation (31) compared to two other integration schemes for a 3D ME rail model subjected to a precalculated contact force and for a complete wheelset/track interaction model, respectively. Section 4.3 presents the potencialities of the linearised interaction model.

### 4.1 Results for a 3D ME rail model subjected to a prescribed contact force

The track is represented by a 3D ME rail model supported by a uniform viscoelastic Winkler bedding in which the vertical bed stiffness and damping values equivalent to discrete rail supports are gathered in Table 1. The values for the longitudinal and lateral directions are modelled as the 10% and 80% of the vertical ones, respectively. The UIC60 profile is extruded along 42 m, resulting a solid mesh of 8452 solid quadratic elements with a total of 170175 degrees of freedom. The models consists of an

adaptive longitudinal mesh in which the element length increases linearly from the central element to 60% of the half-length of the rail on each side, while the remaining 40% presents uniform element lengths. The central element length is 1 cm. A mode shape functions matrix with 2000 mode shapes is computed, covering a frequency range up to 8.5 kHz.

In the direction of making a first approximation to the computational performance of the decoupling solver, the simulations are carried out for one 3D ME rail model without considering the interaction with the wheel through the contact. The following study is focused on the rolling contact phenomenon with the wheel/rail roughness as external excitation, in line with the work carried out by Li *et al.* for a simply supported beam but using an adaptive algorithm in the time domain[11]. With this purpose, it is used a prescribed contact force applied in the contact node that has been previously calculated from a simulation in a tangent and randomly corrugated rail, assuming a corrugation spectrum corresponding to the ISO 3095 limit[26], which establishes a third-octave band spectrum of the rail roughness. A first simulation is run for the maximum number of modes for the rail model (2000 modes); the *ode45* solution will be used as reference one to compute the discrepancies between approaches later. Figure 5 plots the computed vertical displacement of the contact node along 0.2 s (instead of the 1 s simulated to a better visualisation) using the three integration schemes mentioned. As observed, the three methods obtain similar results and capture the same behaviour in relation to the roughness excitation introduced. The zoomed view points out that the decoupling method fits better the *ode45* reference solution than the Newmark algorithm, a first indicator of the computational advantages of the proposed scheme.

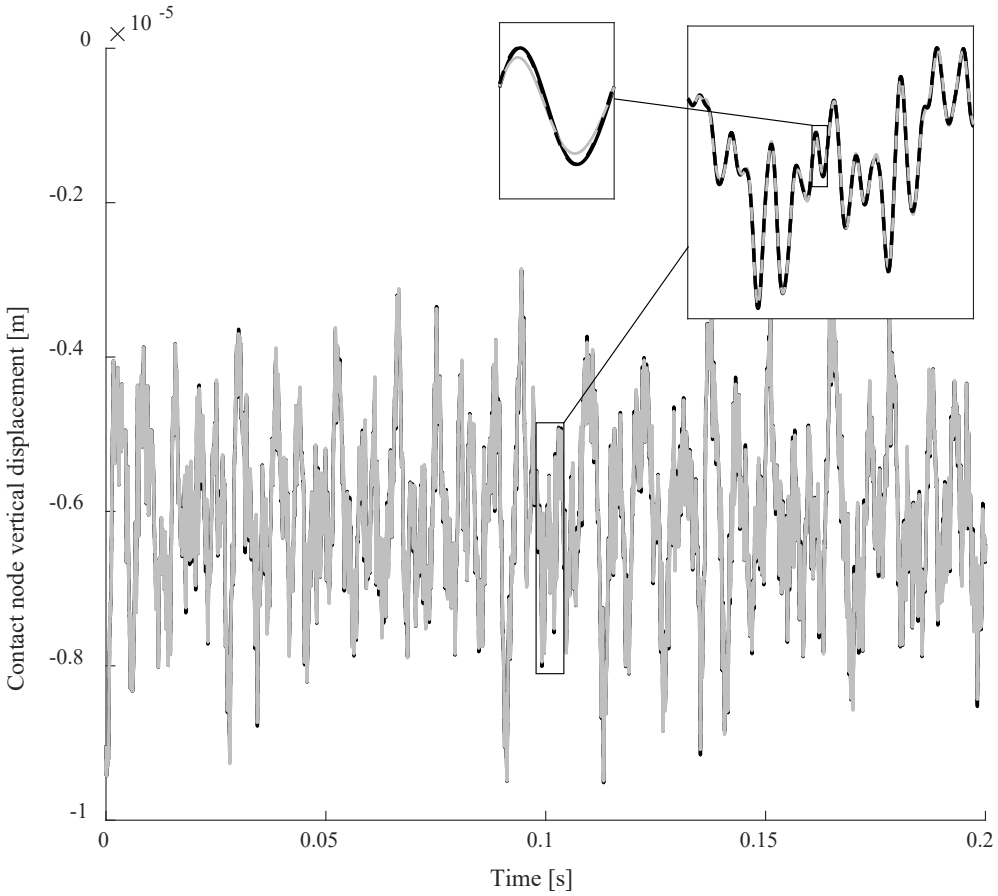


**FIGURE 5** Time series for the vertical displacement of the contact node of a 3D ME rail model using three schemes of integration: decoupling technique (▬▬), Newmark (▬▬) and *ode45* (- - -)

The computational performance of the three schemes are now evaluated and compared. The simulations are run for different number of modes by truncating the mode shape functions matrix previously computed for the rail model. Increments of 40 modes are considered, selecting square matrices of this dimension from the reference matrix of 2000 modes; in total, 50 cases are run for each scheme. The computational time required for a simulation time of 1 s and the discrepancy computed from the reference solution are gathered for each simulation and plotted in Figures 6. Figure 6(a) shows that both constant-step decoupling and Newmark schemes reduce drastically the time consumption required for the simulation compared with the *ode45* scheme. It is observed that the decoupling method requires lower computational times than Newmark (82.5 vs. 114.6 s for 2000 modes) without compromising the accuracy of the solution as seen in Figure 6(b): the three schemes follows a similar decreasing curve with the number of modes. Figure 6(c) synthesises the previous figures, showing that the decoupling technique permits to reach an accurate solution for lower computational times, then enhancing the numerical efficiency of the time integration.

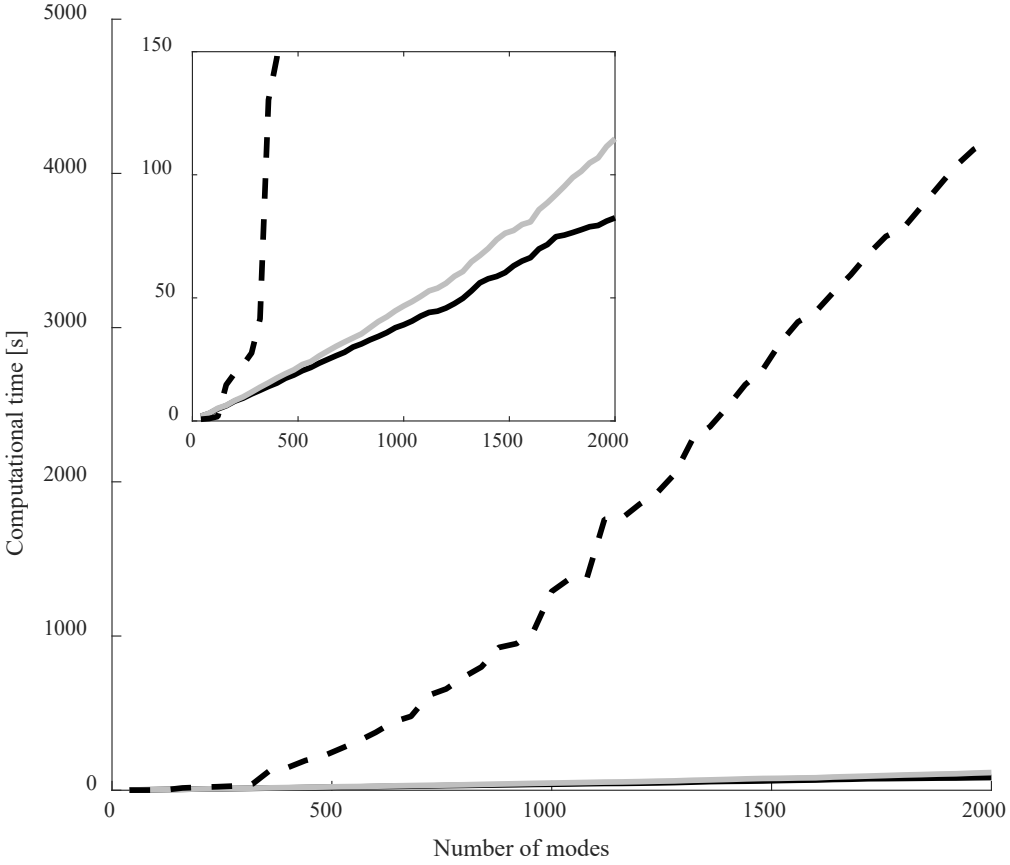
5000
4000
3000
2000
1000
0
Computational time [s]
0
500
1000
1500
2000
Number of modes
150
100
50
0
0
500
1000
1500
2000

**(a)**

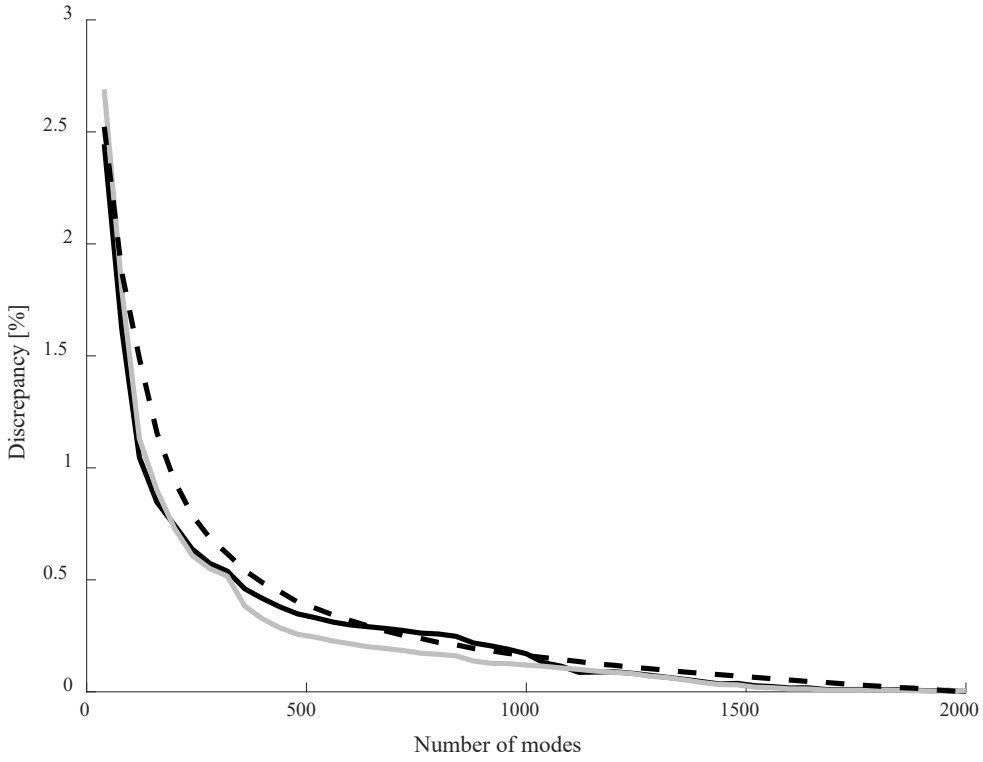
3
2.5
2
1.5
1
0.5
0
Discrepancy [%]
0
500
1000
1500
2000
Number of modes

**(b)**

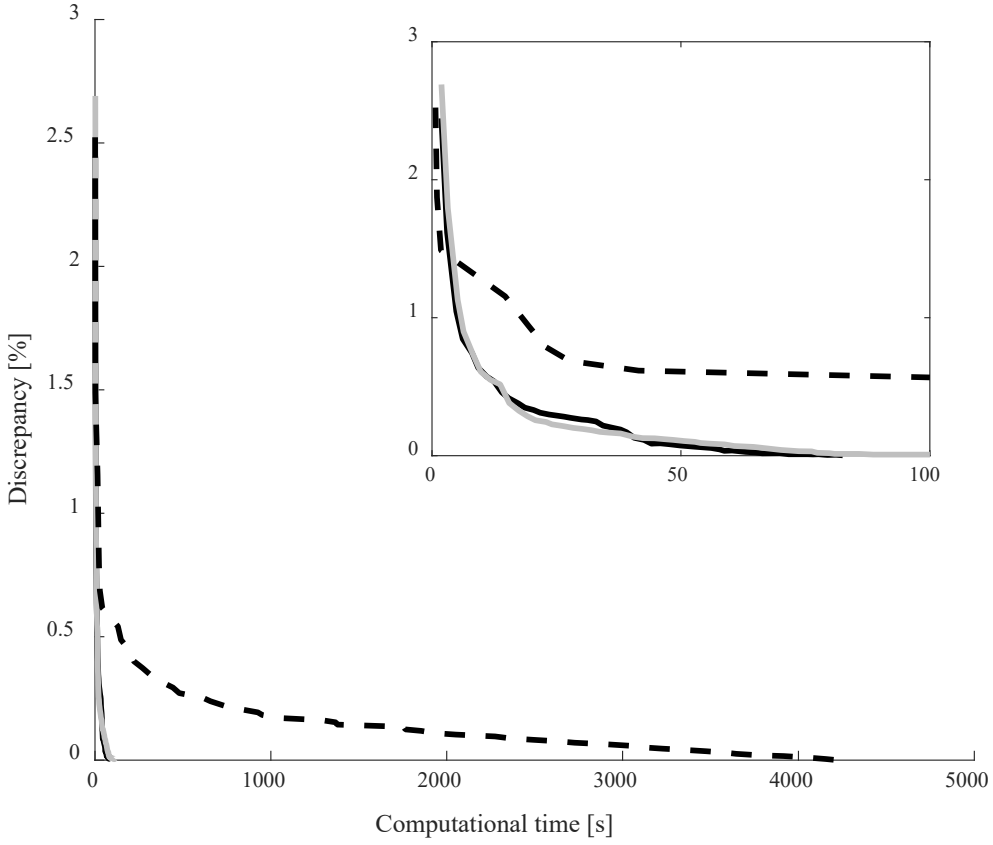


**(c)**

**FIGURE 6** Comparison of the computational performance of the numerical integration of a 3D ME track model subjected to a precalculated contact force applied in the contact node through the decoupling (▬▬), Newmark (▬▬) and *ode45* (▬ ▬ ▬) schemes. (a) Number of modal coordinates vs. computational time required for a simulation time of 1 s; (b) number of modal coordinates vs. discrepancy with respect to the reference solution; (c) computational time vs. discrepancy

### 4.2 Results for the wheelset/track interaction model

The wheelset is incorporated to the following simulation. Two rails are now considered to interact with both wheels of the wheelset. The interaction model corresponding to Equation (17) is solved for tangent and randomly corrugated rails, assuming a corrugation spectrum defined by the ISO 3095 limit. In this case, the normal and tangential contact forces are computed through an instationary and non-linear contact model based on Kalker's variational theory[22] with a potential contact area discretised into 20×20 boundary elements. The spatial resolution for the mesh of the potential contact area considered is 0.25 and 1 mm in longitudinal and lateral directions, respectively. This refinement permits to capture the contact dynamics arisen for high-frequency phenomena such as the rolling

contact under study, hence introducing an additional high-consuming computational work that abruptly increases the required computational time[25].

The wheelset model is meshed with 12340 solid quadratic elements (20-nodes) and includes a total of 260145 degrees of freedom. A mode shape functions matrix with 400 mode shapes is computed for the wheelset model, covering a frequency range up to 8.5 kHz. The reference solution is computed for 400 vibration modes for the wheelset and 2000 modes for both rails, thus handling a problem dimension of 4800 unknowns. The simulations are run for different number of modes by truncating the mode shape functions matrix previously computed for the wheelset and the rail. Increments of 8 modes are considered for the wheelset and 40 modes for the rail, selecting square matrices of the corresponding dimensions from the reference matrices of 400 and 2000 modes for the wheelset and the track (both rails), respectively; in total, 50 cases are run for each scheme up to 4400 modes. The time simulated is 1 s. Figure 7 plots the computed vertical displacement of the contact node along the simulation time using the three integration schemes, which give approximate results in line with the previous observations.

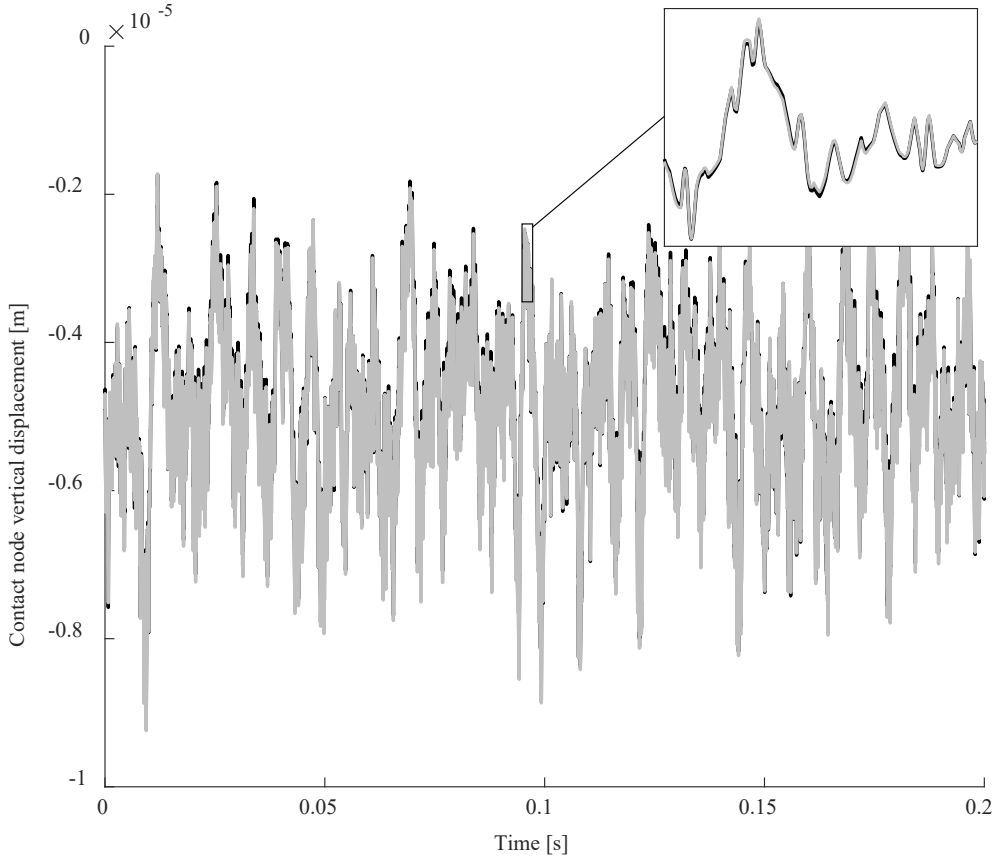


**FIGURE 7** Time series for the vertical displacement of a contact node of a wheelset/track interaction model using three schemes of integration: decoupling technique (▬▬), Newmark (▬▬) and *ode45* (- - -)

*ode45* was run only once in a PC with better computer specifications to get the reference solution shown above; its evaluation for different number of modes with the conventional PC used in the first set of simulations was unadressable, so only the decoupling and Newmarck schemes are run in this section. The increase of the system dimension and the need of the resolution of the contact algorithm involve much larger times (hours) as seen in Figure 8(a). It is observed a better performance of the decoupling integration, more significant than the results gathered in Figures 6 as expected for a more complex system with larger dimension. Its computational velocity is 2.4 times faster than Newmark again without compromising the discrepancy as seen in Figure 8(b). This numerical behaviour is summarised in Figure 8(c), which shows how the decoupling algorithm reduces to zero the discrepancy associated with the truncation for 4.5 h while Newmark method needs 10.6 h. These results are in agreement with Section 4.1, thus revealing the proposed algorithm as a more efficient constant-step integration method than the Newmark scheme.

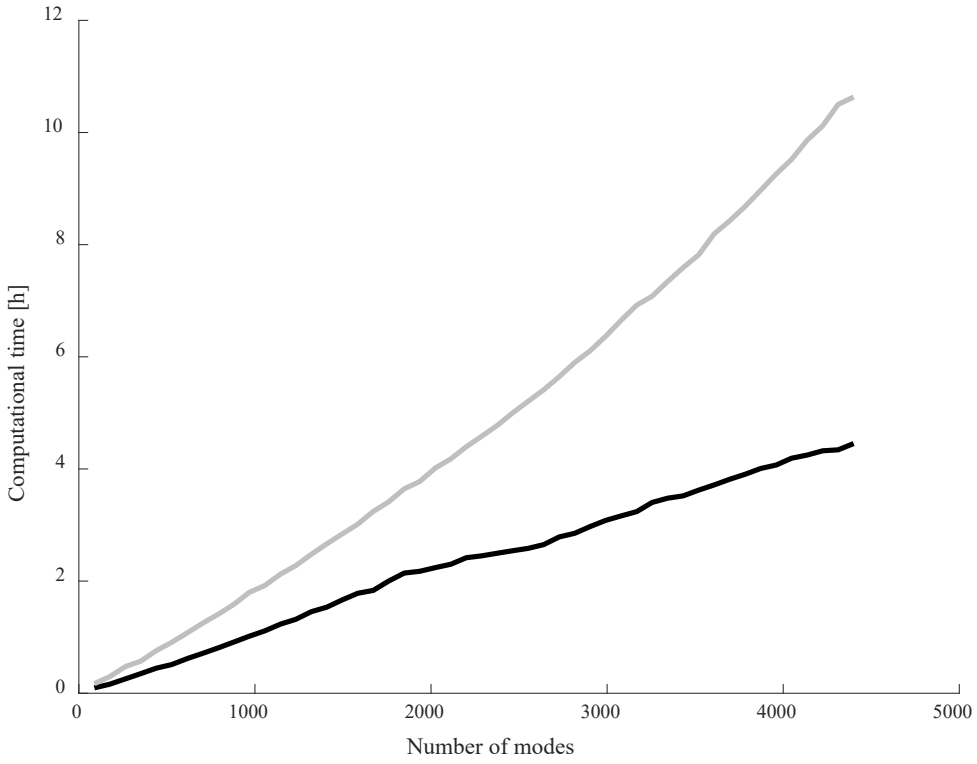


**(a)**

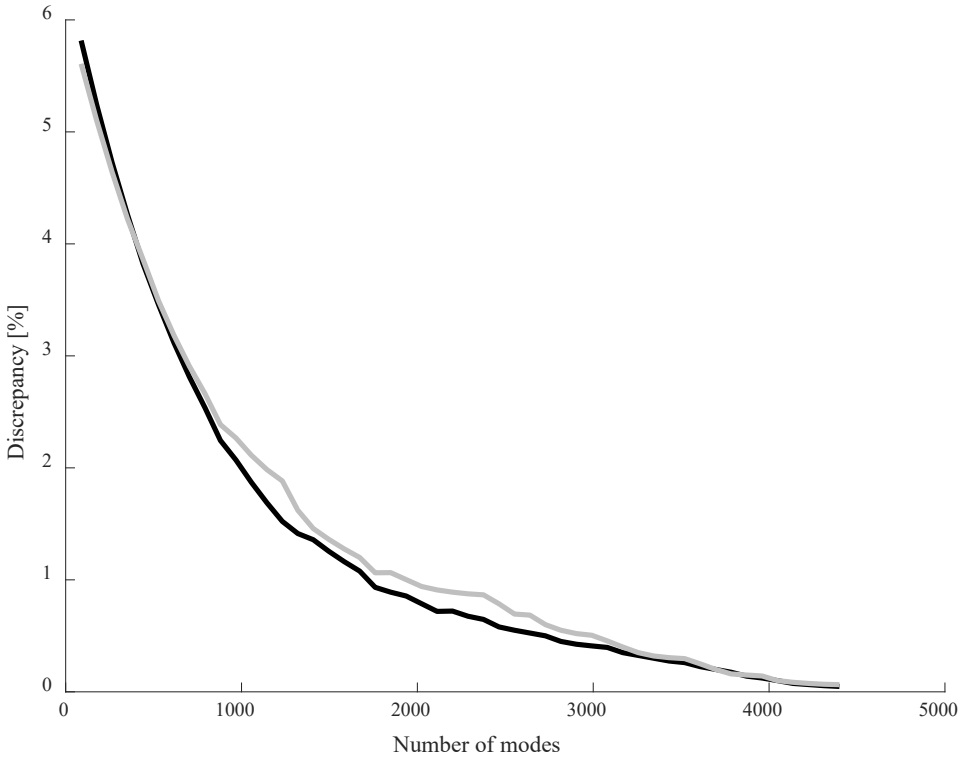
Discrepancy [%]
Number of modes
0
1
2
3
4
5
6
0
1000
2000
3000
4000
5000

**(b)**

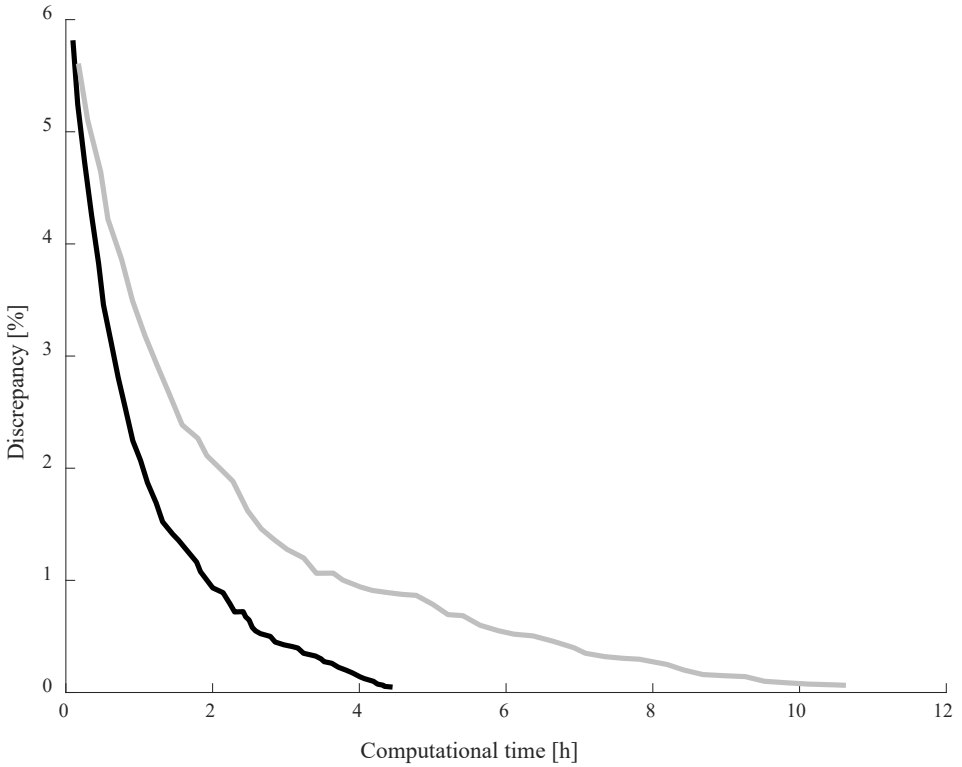
Discrepancy [%]
Computational time [h]
0
1
2
3
4
5
6
0
2
4
6
8
10
12

**(c)**

**FIGURE 8** Comparison of the computational performance of the numerical integration of the complete wheelset/track dynamic interaction model through the decoupling (━━━) and Newmark (━━━) schemes. (a) Number of modal coordinates vs. computational time required for a simulation time of 1 s; (b) number of modal coordinates vs. discrepancy with respect to the reference solution; (c) computational time vs. discrepancy

### 4.3 Linearised interaction model

The computational potentialities of the linearised model described in Section 3.3 are now under study. Figure 9(a) shows the time series of the normal contact force corresponding to one wheel, computed through: (1) the numerical integration of the complete non-linear interaction model; (2) the analytic solution given by the linearised interaction model deduced in Equation (41). It is observed that both models give a mean value about 40 kN and amplitudes of similar order for the case studied. As expected, Figure 9(b) shows that the simplified model is not able to represent well the high-frequency content arisen for the complex boundary-element based contact algorithm used. Nevertheless, it appears as a promising tool for a first insight in preliminary stages with practically no time cost.

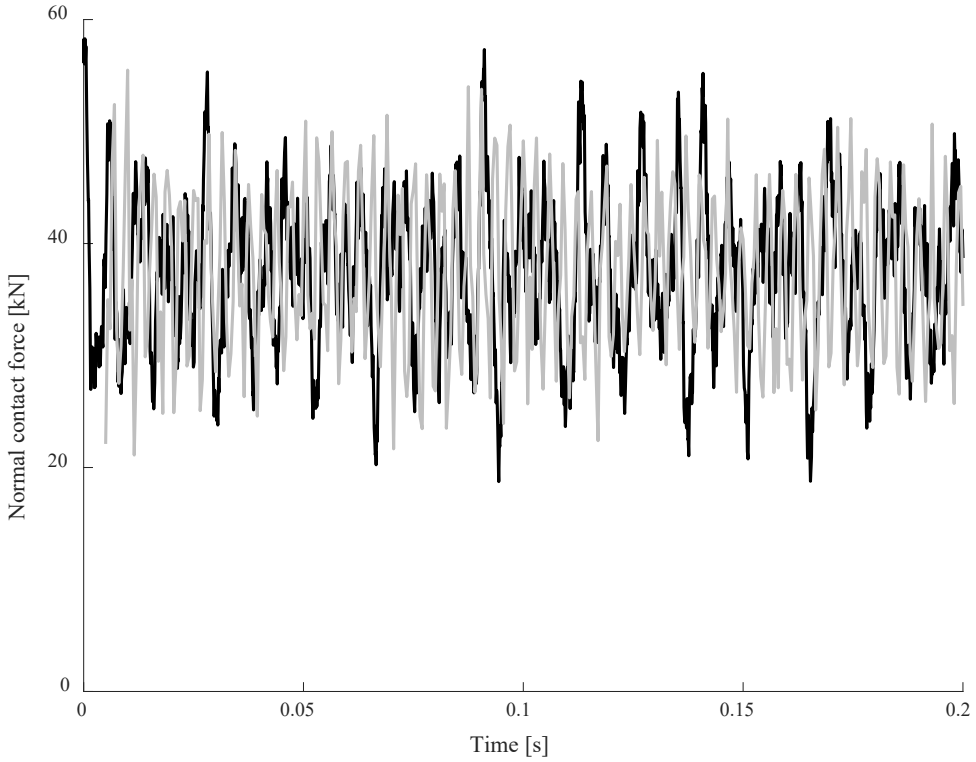


**(a)**

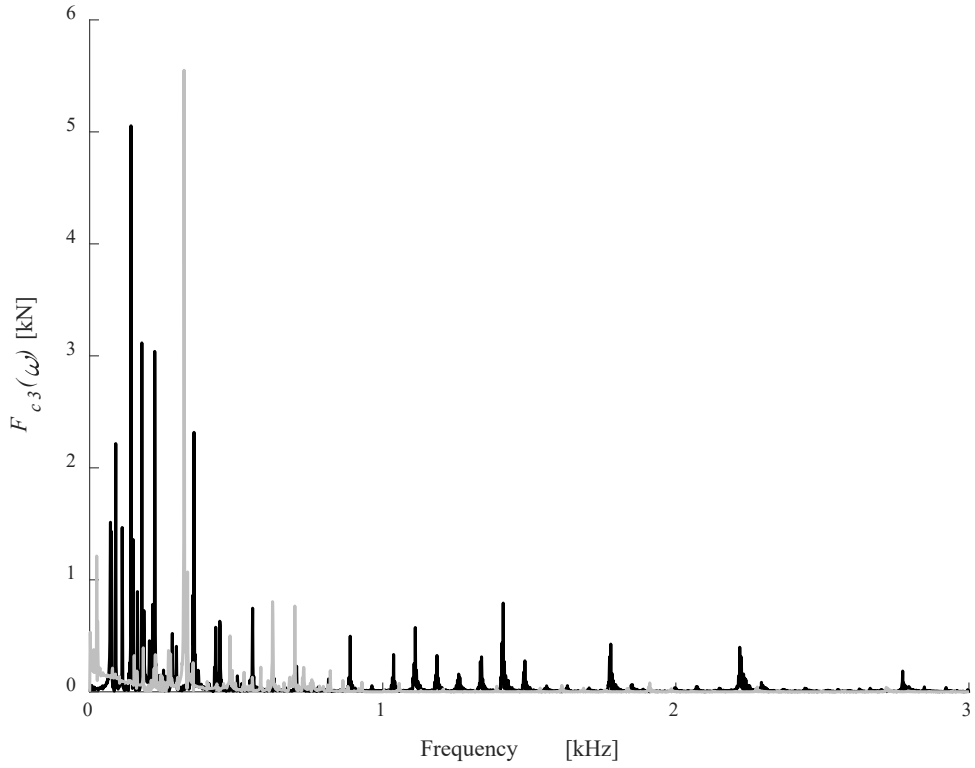


**(b)**

**FIGURE 9** Normal contact force through numerical integration (——) and the linearised interaction model described in Equation (41) (——). (a) Time series; (b) frequency content

As seen in Equation (41), the compact linear formulation includes the contact force terms in the stiffness matrix, so making the resulting matrix equation of motion homogeneous. This leads to an additional and very important numerical advantage: the receptance diagram of the entire wheelset/track system can be computed in contrast to the non-linear model, which are plotted in Figures 10. The first one shows the corresponding direct and cross point receptances at the contact node up to 3 kHz, whereas the second figure evaluates the influence of the wheelset and the track receptances in the wheelset/track system in the vertical point receptance. The linearised model also enables to get the mode shape of the wheelset and the rails in contact as a unique system, adding a new potentiality for the developed formulation. Figure 11 represents the mode shape corresponding to the resonance peak marked in Figure 10(b) at 2.1 Hz, where the deformed configuration of the substructures are clearly visualised. It corresponds to an axial mode for the wheelset, in which both wheels present a mode deformed displacement corresponding with an axial disc mode of two nodal diameter and zero nodal circles; the rails show a bending mode for this frequency.

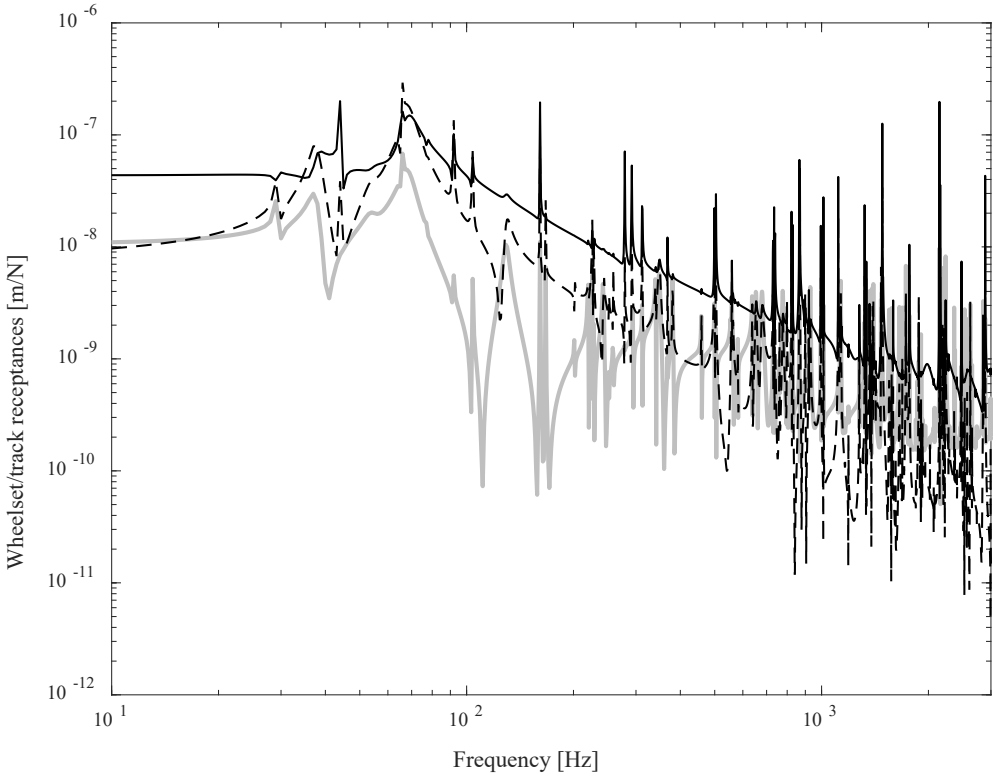
Wheelset/track receptances [m/N]
Frequency [Hz]

**(a)**

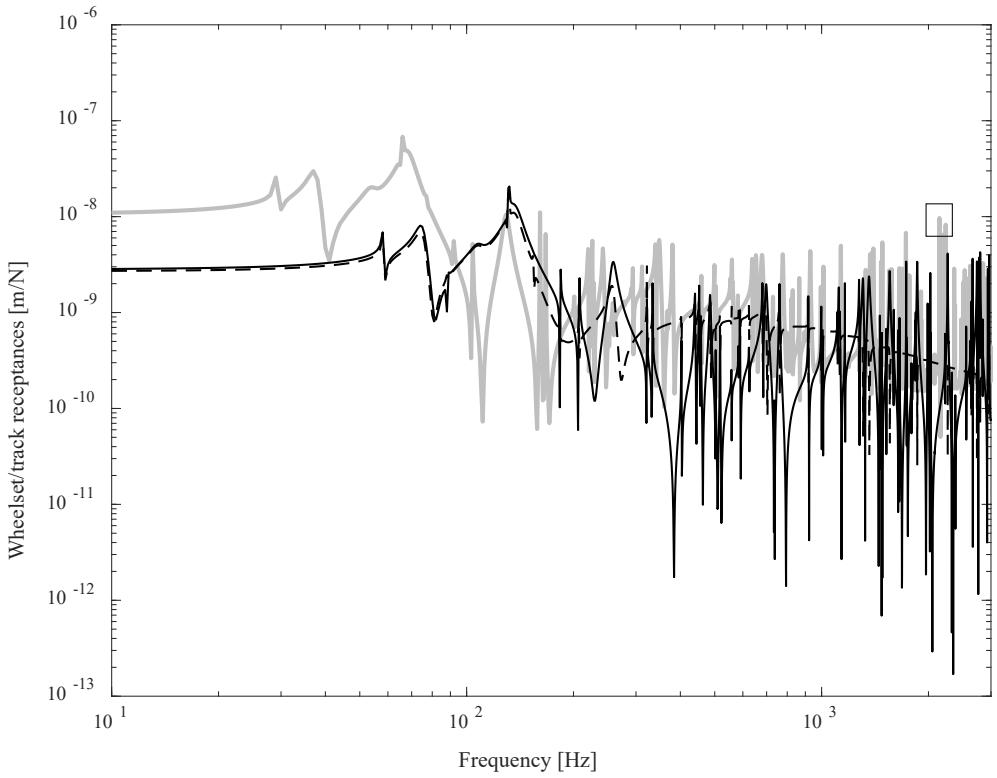
Wheelset/track receptances [m/N]
Frequency [Hz]

**(b)**

**FIGURE 10** (a) Point receptance at the contact node of the linearised wheelset/track interaction model in the vertical (——), lateral (——) and crossing (— —) directions; (b) direct vertical point receptances at the contact node for the interaction (——), wheelset (——) and track (— —) models

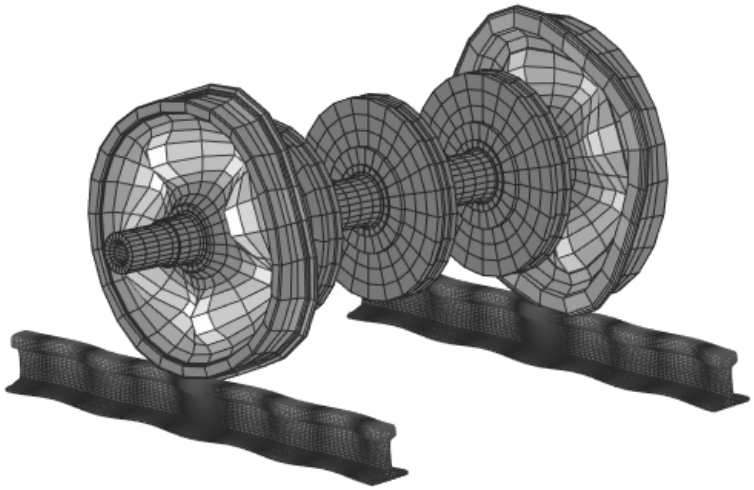

**FIGURE 11** Mode shape configuration for the wheelset/track railway system at the resonance peak corresponding to 2.1 kHz

## 5. CONCLUSIONS

A new scheme of constant time-step integration based on a decoupling technique is proposed in this work for high-frequency railway dynamics. The matrices associated with the equations of motion in modal coordinates are diagonalised through a new modal variable vector, obtaining uncoupled first-order linear differential equations in modal coordinates. Simulations in tangent conditions with head-rail roughness excitation have been run with this scheme for a growing number of modes. Its computational performance has been compared with the constant time-step Newmark and adaptive Runge-Kutta-based *ode45* schemes, widely used in vehicle dynamics. Results show that the decoupling scheme considerably reduces the time consumption of the simulation without compromising the accuracy of the solution. The proposed method is revealed more adequate in terms of efficiency for high-frequency domain problems than generic variable time-step Runge-Kutta methods commonly used in this field. The deduced formulation is extended to a case of linearised wheel/rail contact, permitting to calculate the receptance of the complete wheelset/track system in an efficient way.

## REFERENCES


1. Thompson DJ. *Railway Noise and Vibration: Mechanisms, Modelling and Means of Control*. Oxford, UK: Elsevier; 2009.

2. Nielsen JCO, Lundén R, Johansson A, Vernersson T. Train-track Interaction and Mechanisms of Irregular Wear on Wheel and Rail Surfaces. *Vehicle Syst Dyn*. 2003;40(1-3):3-54.
3. Ekberg A. Fatigue of railway wheels. *In: The Wheel/Rail Interface Handbook Woodhead Publishing in Mechanical Engineering*. 2009; 211-244.
4. Grassie SL, Gregory RW, Harrison D, Johnson KL. Dynamic response of railway track to high frequency vertical excitation. *J Mech Eng Sci*. 1982;24:77-90.
5. Popp K, Kaiser I. Interaction of elastic wheelsets and elastic rails: modelling and simulation, *Vehicle Syst Dyn*. 2006;44(Suppl.):S932-S939.
6. Thompson DJ, Jones CJC. A Review of the Modelling of Wheel/Rail Noise Generation. *J Sound Vib*. (2000;231(3):519-536.
7. Baeza L, Fayos J, Roda A, Insa R. High frequency railway vehicle-track dynamics through flexible rotating wheelsets. *Vehicle Syst Dyn*. 2008;46(7):647-662.
8. Martínez-Casas J, Fayos J, Denia FD, Baeza L. Dynamics of damped rotating solids of revolution through an Eulerian modal approach. *J Sound Vib*. 2012;331:868-882.
9. Vila P, Baeza L, Martínez-Casas J, Carballeira J. Rail corrugation growth accounting for the flexibility and rotation of the wheel set and the non-Hertzian and non-steady-state effects at contact patch. *Vehicle Syst Dyn*. 2014;52:92-108.
10. Hosking RJ, Milinazzo F. Floating ladder track response to a steadily moving load. *Math Method Appl Sci*. 2007;25:1823-1841.
11. Li H, Yang H, Li N, Alonso A. An adaptive algorithm in time domain for dynamic analysis of a simply supported beam subjected to a moving vehicle. *Math Method Appl Sci*. 2011;34:996-1005.
12. Koh CG, Ong JSY, Chua DKH, Feng J. Moving Element Method for train-track dynamics. *Int J Numer Meth Eng*. 2003;56:1549-1567.
13. Torstensson PT, Nielsen JCO, Baeza L. Dynamic train-track interaction at high vehicle speeds-Modelling of wheelset dynamics and wheel rotation. *J Sound Vib*. 2011;330:5309-5321.
14. Newmark NM. A method of computation for structural dynamics. *J Eng Mech-ASCE*. 1959;85(EM3):67-94.
15. Shampine LF, Reichelt MW. The MATLAB ODE Suite, *SIAM J Sci Comput*. 1997;18:1-22.
16. Baeza L, Ouyang H. A railway track dynamics model based on modal substructuring and cyclic boundary condition. *J Sound Vib*. 2011;330:75-86.
17. Baeza L, Roda A, Nielsen JCO. Railway vehicle/track interaction analysis using a modal substructuring approach. *J Sound Vib*. 2006;293:112-124.
18. Martínez-Casas J, Mazzola L, Baeza L, Bruni S. Numerical estimation of stresses in railway axles using a train–track interaction model. *Int J Fatigue*. 2013;47:18-30.
19. Martínez-Casas J, Giner-Navarro J, Baeza L, Denia FD. Improved railway wheelset-track interaction model in the high–frequency domain. *J Comput Appl Math*. 2017;309:642-653.

20. Hertz H, Ueber die Berührung fester elastischer Körper. *J reine ange Math*. 1882;92:156-171.
21. Pieringer A, Torstensson PT, Giner-Navarro J, Baeza L. Investigation of railway curve squeal using a combination of frequency- and time-domain models. *Proc 12th IWRN*. 2016;444-451.
22. Kalker JJ. *Three-Dimensional Elastic Bodies in Rolling Contact*. Dordrecht, The Netherlands: Kluwer; 1990.
23. Mazzola L, Bezin Y, Bruni S. Vehicle-Track interaction: MB simulation for track loading limits and damage identification. *ECCOMAS Them Conf Multibody Dyn*: Brussels, Belgium; 2011.
24. Giner-Navarro J, Baeza L, Vila P, Alonso A. Study of falling friction effect on rolling contact parameters. *Tribol Lett*. 2017;65:29.
25. Giner-Navarro J, Martínez-Casas J, Denia FD, Baeza L. Study of curve squeal in the time domain using an advanced high-frequency train/track interaction model. *J Sound Vib*. 2018;431:177-191.
26. ISO 3095:2005. *Railway applications. Acoustics. Measurement of noise emitted by railbound vehicles*. CEN: Brussels, Belgium; 2005.

**TABLE 1** Simulation parameters and properties

| **Wheelset model data** | | **Track model data** | |
|---|---|---|---|
| Mass of wheelset | 1375 kg | Rail section | UIC60 |
| Axle load | 120 kN | Rail length | 42 m |
| Primary suspension longitudinal stiffness | 7.5 MN/m | Track vertical bed stiffness | 43.7 MN/m |
| Primary suspension lateral stiffness | 7.1 MN/m | Track vertical bed damping | 12.6 kN s/m |
| Primary suspension vertical stiffness | 0.81 MN/m | | |
| Primary suspension longitudinal damping | 100 kN s/m | | |
| Primary suspension lateral damping | 100 kN s/m | | |
| Primary suspension vertical damping | 30 kN s/m | | |

## FIGURE CAPTIONS

**FIGURE 1** Reference frames and position vectors. The undeformed configuration of the wheelset is shown in dashed trace; a generic position of the flexible wheelset is sketched in solid colours

**FIGURE 2** Finite element mesh of the UIC60 rail (out of scale). Deformed and undeformed configuration

**FIGURE 3** Reference system used in the contact

**FIGURE 4** Vertical displacement of the central node on the upper side of the 1D ME rail model. Results from: physic coordinates, 200 nodes (– – –); modal coordinates, 50 modes (———); modal coordinates, 50 modes, and compensated by the static modal correction $\mathcal{G}$ (———)

**FIGURE 5** Time series for the vertical displacement of the contact node of a 3D ME rail model using three schemes of integration: decoupling technique (———), Newmark (———) and *ode45* (– – –)

**FIGURE 6** Comparison of the computational performance of the numerical integration of a 3D ME track model subjected to a precalculated contact force applied in the contact node through the decoupling (———), Newmark (———) and *ode45* (– – –) schemes. (a) Number of modal coordinates vs. computational time required for a simulation time of 1 s; (b) number of modal coordinates vs. discrepancy with respect to the reference solution; (c) computational time vs. discrepancy

**FIGURE 7** Time series for the vertical displacement of a contact node of a wheelset/track interaction model using three schemes of integration: decoupling technique (———), Newmark (———) and *ode45* (– – –)

**FIGURE 8** Comparison of the computational performance of the numerical integration of the complete wheelset/track dynamic interaction model through the decoupling (———) and Newmark (———) schemes. (a) Number of modal coordinates vs. computational time required for a simulation time of 1 s; (b) number of modal coordinates vs. discrepancy with respect to the reference solution; (c) computational time vs. discrepancy

**FIGURE 9** Normal contact force through numerical integration (———) and the linearised interaction model described in Equation (41) (———). (a) Time series; (b) frequency content

**FIGURE 10** (a) Point receptance at the contact node of the linearised wheelset/track interaction model in the vertical (———), lateral (——) and crossing (— —) directions; (b) direct vertical point receptances at the contact node for the interaction (———), wheelset (——) and track (— —) models

**FIGURE 11** Mode shape configuration for the wheelset/track railway system at the resonance peak corresponding to 2.1 kHz